Tanzania Journal of Science 50(5): 1028-1044, 2024
ISSN 0856-1761, e-ISSN 2507-7961
© College of Natural and Applied Sciences, University of Dar es Salaam, 2024

Single-step sol-gel synthesis of CuO/TiO_2 nanoparticles: Microstructure and materials characterization

Godlisten N Shao
Department of Chemistry, Mkwawa University College of Education, University of Dar es Salaam, P.O. Box 2513, Iringa, Tanzania
godlisten.shao@udsm.ac.tz/shaogod@gmail.com
Received 31 Oct 2023, Revised 21 July 2024, Accepted 14 Oct 2024, Published 31 Dec 2024
https://dx.doi.org/10.4314/tjs.v50i5.11

Abstract

Copper oxide modified titanium dioxide (CuO/TiO_2) nanoparticles have been widely reported owing to their excellent performance in heterogeneous photocatalysis. However, their industrial and large-scale production is hampered by tedious and expensive preparation methods. The present study presents a single step sol-gel synthesis of CuO/TiO_2 nanoparticles with improved physicochemical properties. A series of CuO/TiO_2 nanoparticles were synthesized by a modified sol-gel approach using titanium oxychloride as a TiO_2 precursor in the absence of additives. The samples were examined by high-resolution TEM, SEM-EDAX, XRD, XRF, XPS, Raman spectroscopy, nitrogen gas physisorption studies, and UV-visible DRS analyses. It was found that the proposed method facilitated the formation of CuO/TiO_2 nanoparticles with superior morphology, crystal structure and optical properties. XRD results showed that the introduction of Cu^{2+} into TiO_2 microstructure delayed the anatase to rutile phase transformation in the calcined samples. Hence, samples with pure anatase phase, pure rutile phase or a mixture of anatase and rutile TiO_2 phases were exquisitely yielded. The band gap energy of the TiO_2 was reduced from 3.14 eV to ~ 2.0 eV due to the presence of CuO. Therefore, the present study provides a convenient method to yielding sol-gel synthesized CuO/TiO_2 with improved physico-chemical properties in the absence of additives.

Keywords: Microstructure; Sol-gel process; Copper oxide-titania nanoparticles; Calcination.

Introduction

Titanium dioxide (TiO_2) is the most important n-type semiconductor with remarkable applications due to its fascinating thermal, electrochemical and optical properties (Comini et al. 2009, Nakata and Fujishima 2012, Li et.al 2014, Abidi et al. 2020). It occurs in three different polymorphic structures namely anatase, brookite or rutile phases with the metastable anatase and brookite transform into the thermodynamically stable rutile upon sintering at high temperatures. The wide band gap of TiO_2 (E_g=~3.0-3.3 eV) and its rapid recombination of the photogenerated electron–hole pairs in single phased semiconductor can adversely hamper its performances. This drawback can be overcome through three strategies: (i) formation of TiO_2 products with mixed phases; (ii) formation of binary systems/composites such as ZnO/TiO_2, CuO/TiO_2, ZrO_2/TiO_2, SiO_2/TiO_2, NiO/TiO_2, WO_3/TiO_2; and (ii) doping TiO_2 with metals or nonmetals (Hanaor and Sorrell 2011, Pelaez et al. 2012, Moniz and Tang 2015, Mutuma et al. 2015; Tan et al. 2016).

Meanwhile, CuO/TiO_2 binary metal oxide semiconductor are useful materials in heterogeneous photocatalysis, hydrogen gas production and solar cell technology due to their unique electronic and optical attributes (Moniz and Tang 2015, Baig et al. 2020, Baran et al. 2022). CuO is chemically and

thermally stable oxide with band gap energy of 1.2-2.6 eV depending on the preparation conditions. The ionic radius of Ti^{4+} (0.65 Å) and Cu^{2+} (0.68 Å) are very comparable hence their oxides can be blended to form composites (Xu et al. 2018, Prajapat et al. 2024). The introduction of the Cu^{2+} into the TiO_2 microstructure is thought to create sub-band states in the band gap of TiO_2 leading to band gap reduction. This leads to subsequent extension of the absorption edge of TiO_2 to the UV-visible region. Various studies propose that the existence of Cu^{2+} in TiO_2 causes the bending of the conduction and valence bands due to formation of grain boundary defects (Choudhury et al. 2013; Prajapat et al. 2024). Thus, Cu^{2+} can act as electrons scavenger to hamper the recombination of the electron-hole pairs. Indeed, phase transformation and morphology of the final products can also be altered through modification of TiO_2 with CuO as well (Anpo and Takeuchi 2003, Choudhury et al. 2013, Clarizia et al. 2014, Lin et al. 2018). Hence, designing suitable synthetic methods that consume less-expensive precursors is of great interest. This can essentially provide flexibility in producing CuO/TiO_2 nanoparticles with unique properties for various applications.

To date, there are various preparation methods that are used in the preparation of the CuO/TiO_2 nanoparticles with promising physico-chemical properties (crystal structure, morphology and absorption in the UV-visible region). These include photodeposition, pulsed laser ablation in liquid, hydrothermal, sol-gel, chemical vapor deposition, co-precipitation, ball milling, spray pyrolysis methods, solvothermal and so on (Zaleska 2008, Clarizia, et al. 2014, Moniz and Tang 2015, Shao et al. 2015, Etape et al. 2017, Baig et al. 2020, Thongpool et al. 2020). Among these methods, the sol-gel process is customarily adopted due to its cost-effectiveness and versatility in producing homogeneous products at desirable conditions (Clarizia et al. 2014, Zeng et al. 2017, Thongpool et al. 2020). The sol-gel method can enhance large-scale production and commercialization of CuO/TiO_2 semiconductors especially when the employed preparation method is simple and consumes less expensive precursors. Customarily, the industrial and large-scale production of CuO/TiO_2 is hampered by the consumption of high-cost precursors, tedious preparation steps, and the requirement for hydrothermal treatment which requires expensive autoclaves operated at high temperatures and pressures (Moniz and Tang 2015, Zeng et al. 2017, Baig et al. 2020). Baig et al. (2020) reported a single step production of high-purity CuO/TiO_2 nanocomposites using pulsed laser ablation in liquid (PLAL) approach. Regardless of the uniqueness of the PLAL method, the employed preparation process consumed pure CuO and pure TiO_2 as precursors. Zeng et al. (2017) used the sol-gel method to synthesize CuO/TiO_2 with high dispersion of CuO species. The study used tetrabutyl titanate (titanium alkoxide) as a TiO_2 precursor. Ravishankar et al. (2020) prepared CuO/TiO_2 nanocomposite photocatalysts through a surfactant-assisted sol–gel method using titanium (IV) isopropoxide as a TiO_2 precursor. In that report hexadecyltrimethylammonium bromide was added to act as a structure directing agent to control the morphology of the formed CuO/TiO_2 nanocomposites. These reports reveal that the consumption of additives, pure metal oxides or metal alkoxide precursors can hamper the industrial and large-scale production of CuO/TiO_2 nanocomposites. Thus, there is the need to envisage facile and controllable preparation methods that preclude the consumption of additives, expensive precursors and tedious preparation methods.

Previously, $TiOCl_2$ solution was used for the preparation of metal oxide systems with promising properties for various applications (Shao et al. 2012, Shao et al. 2012a, Kim et al. 2013, Shao et al. 2013). It was found that the use of the $TiOCl_2$ solution as a TiO_2 precursor yields final products with high TiO_2 loadings and less-aggregated particles. However, in those aforementioned reports a two-step sol-gel preparation method was used to produce the final products. Despite the

uniqueness of the two-step sol-gel route, the cost of production can largely be reduced by employing a convenient single-step sol-gel method to produce metal oxide systems with appealing physico-chemical properties. Herein, a controllable, versatile and reproducible single-step sol-gel method was used to synthesize CuO/TiO_2 nanoparticles with controlled phase structure, morphology and optical properties. Titanium oxychloride solution (which is a rarely used TiO_2 precursor) was used as a TiO_2 source. The main merit of the proposed method is that the process is facile and convenient to adopt whilst the TiO_2 precursor used herein is relatively cheap and facilitates the formation of CuO/TiO_2 nanoparticles in the absence of additives. There are a few reports (Yuan et al. 2018, Baig, et al. 2020) investigated the influence of CuO on the microstructure of TiO_2-based materials. However, no study has provided a comparison using the synthetic method and TiO_2 precursor suggested by the present study.

Materials and method

$TiOCl_2$ (25 wt.%) was purchased from Kukdong Chemicals Co. Ltd, Korea Republic while ammonium hydroxide solution (28%) was bought from Dae-Jung Chemical and Metal Co. Ltd, Korea Republic. Copper (II) acetate (98%) was acquired from Sigma-Aldrich. The chemical reagents used in the present study were purchased from commercial sources and used without further purification. A single step sol-gel process was used to prepare CuO/TiO_2 samples in the absence of additives. In these particular experiments, both 3.125 mmol copper (II) acetate and 50.0 mmol titanium oxychloride precursors were added into a beaker containing 200 mL of de-ionized water. The mixture was stirred for 4 h to obtain a homogeneous solution. The pH of the solution was adjusted using ammonium hydroxide to 9.0 to obtain slurry. The temperature of the reactor was raised from room temperature to 90 ℃ for 6 h to enhance aging. After 6 h the temperature of the slurry was lowered to room temperature and the product was recovered by vacuum filtration and dried at 100 ℃ for 5 h. The obtained sample was dubbed CT1-00. The same experimental procedures were performed by varying the amount of the copper (II) acetate to 6.25, 12.5, and 25.0 mmol in order to investigate the influence of CuO in the TiO_2 microstructure. The obtained samples were labelled CT2-00, CT3-00 and CT4-00, respectively. The dried samples were calcined in a box furnace at different temperatures ranging from 450 to 800 ℃ for 2 h in an air atmosphere. The calcined samples were dubbed CT-calcination temperature. For example, the sample calcined at 600 ℃ was dubbed CT1-600. XRF analysis of the dried CT4-600, CT3-600, CT2-600 and CT1-600 samples revealed that the Ti/Cu ratios were approximately 2, 5.7, 11.5, and 16.5, respectively. For the sake of comparison, pure TiO_2 powder was synthesized using the procedures described in our previous study (Shao et al. 2016).

Bulk elemental analysis of the dried samples was recorded by an X-ray fluorescence spectrometer (XRF; XRF-1700, Shimadzu Co., Japan with a detection limit of 10 ppm and depth resolution of up to 10 μm). ZAF corrections (atomic number, Z) were used to determine the molar ratios of the elements present in the samples. An X-ray diffractometer (XRD-6000, Shimadzu) was used to examine the crystal structure of the obtained powder using Cu Kα radiation (λ=1.5406 Å). The accelerating voltage and applied current were 40 kV and 100 mA, respectively. The crystallite size of the sample using the Debye-Scherrer formula $D=K\lambda/\beta Cos\theta$; where K is the Scherrer constant, 0.89; β is the full width at half-width height maximum (FWHM) of the diffraction peaks in radians; λ the X-ray wavelength, 1.5406Å; and θ is the Braggs diffraction angle (Tanemura et al. 2003). RENISHAW (RM 1000) Raman microscope was used to record Raman spectra of the samples using a He-Ne laser beam with wavelength of 632.8 nm. The photoelectron spectra of the samples were examined by an X-ray photoelectron spectrometer (XPS; UVS-20-A, SPECS, Germany) using Al Kα X-ray source. The diffuse reflectance spectra

(DRS) of the samples were studied by a UV-visible spectrophotometer (Shimadzu, UV-2600) between 200 and 900 nm using $BaSO_4$ as a reference.

The Brunauer–Emmett–Teller (BET) surface area and the porosity measurements of the samples were studied by a nitrogen gas adsorption-desorption instrument. All of the samples were degassed at 200 ℃ for 2 h prior to actual measurements. The pore size distribution (PSD) and specific desorption pore volumes were obtained using the Barrett-Joyner-Halenda (BJH) method, and desorption branches were used to determine the PSD. The morphology of the samples was investigated by a field-emission scanning electron microscope (FE-SEM, Hitachi S-4800 Japan) with an accelerating voltage of 15.0 kV. The FE-SEM was coupled with energy dispersive spectroscope (EDAX) to determine the purity and elemental composition of the samples. High-resolution transmission electron microscope (HR-TEM, Jeol JEM 2100F-Korea) was used to study the particle size and crystalline structure of the samples.

Results and discussion

The XRD patterns of the as-prepared samples and samples calcined at 450, 600 and 800 ℃ are compiled in Figure 1A-D. It can be seen that the samples displayed various phase structures depending on the amount of CuO and the calcination temperature. Figure 1A shows that the as-prepared TT00 sample displayed broad peaks signifying its amorphous nature. The CuO/TiO_2 samples reveal the presence of anatase TiO_2 crystals. In addition to the anatase phase, the CT4-00 (with high Cu content) shows the existence of peaks for $Cu(OH)_2$ at 16.1^0, 32.3^0 and 39.7^0. This implies that sintering of the as-prepared samples facilitated the transformation of the $Cu(OH)_2$ to CuO (Singh, Ojha, & Srivastava, 2009). Figure 1B-D reveal that the calcined samples displayed different diffractograms signifying that the crystal structure of the samples was dependent on the calcination temperature. Samples calcined at 450 and 600 ℃ show the formation of anatase TiO_2 crystals. The peaks for anatase TiO_2 crystals can be seen at ~25º, 38º, 48º and 56º (Chiarello et al 2008, Shao et al. 2015, Shao et al 2015a). Generally, anatase is the metastable phase of TiO_2 that transforms irreversibly to rutile in air at ~600 ℃ (Hanaor and Sorrell 2011). In addition to the formed TiO_2 crystals, CT3-600 and CT4-600 reveal the formation of peaks for CuO at 38.7º, 48.6º and 58.0º. The XRD results show that no peaks for CuO formed in the CT1 and CT2 series which might be due to the low content of CuO in these samples (Yu et al. 2011).

It can further be observed that calcining the samples at 800 ℃ leads to the anatase to rutile phase transformations (ART). The TT-800 and CT1-800 samples demonstrated a complete ART as only peaks for the rutile TiO_2 crystals can be observed. Notable rutile peaks appear at ~27º, 36º, 47º and 54º (Chiarello et al. 2008, Shao et al. 2012a).

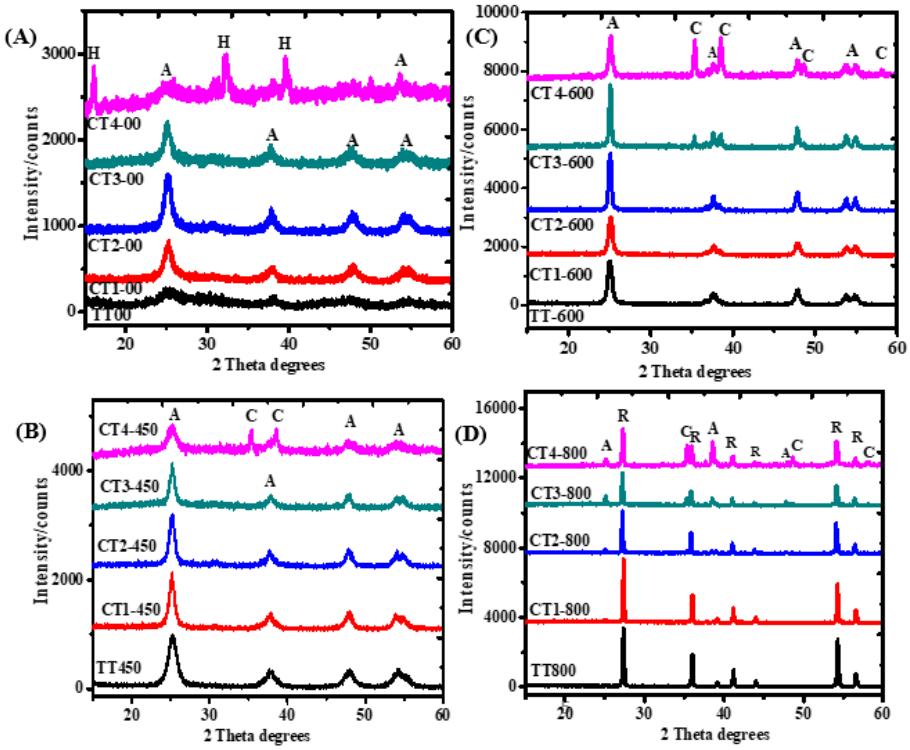

Figure 1: XRD diffractograms of the as-prepared CuO/TiO_2 and calcined samples; as-prepared sample (A), samples calcined at 450 ℃ (B), 600 ℃ (C), and 800 ℃ (D). The peaks for copper hydroxide, copper oxide, anatase and rutile TiO_2 crystals are indicated as H, C, A and R, respectively.

On the other hand, CT2-800, CT3-800 and CT4-800 showed the coexistence of a mixture of anatase and rutile TiO_2 crystals in the CuO/ TiO_2 nanoparticles. This signifies that increasing the amount of CuO in the TiO_2 microstructure delayed the ART. It is worth noting that some peaks for CuO crystals can still be observed in all calcined samples of the CT3 and CT4 series. In addition, the intensities of the XRD peaks increased with increasing the calcination temperature demonstrating that the grain size of the samples and crystallinity were increased as well.

Table 1: Summary of the selected XRD parameters for pure TiO_2 and CuO/TiO_2 nanoparticles

Sample name	2Θ degrees Anatase	2Θ degrees Rutile	2Θ degrees CuO	FWHM Anatase	FWHM Rutile	FWHM CuO	D (nm) Anatase	D(nm) Rutile	D(nm) (CuO)
		-	-		-	-		-	-
TT-450	25.420	-	-	0.674	-	-	12.1	-	-
CT1-450	25.146	-	-	0.862	-	-	9.4	-	-
CT2-450	25.147	-	-	0.809	-	-	10.0	-	-
CT3-450	25.166	-	-	0.716	-	-	11.4	-	-
CT4-450	25.147	-	35.4	1.044	-	0.296	7.8	-	28.1
TT600	25.180	-	-	0.427	-	-	19.0	-	-
CT1-600	25.107	-	-	0.533	-	-	15.3	-	-
CT2-600	25.039	-	-	0.378	-	-	21.5	-	-
CT3-600	25.066	-	35.315	0.280	-	0.215	29.0	-	38.7
CT4-600	25.108	-	35.357	0.472	-	0.305	17.2	-	27.3

TT-800	-	27.360	-	-	0.199	-	-	41.0	-
CT1-800	-	27.360	-	-	0.135	-	-	60.5	-
CT2-800	25.042	27.207	-	0.196	0.162	-	41.5	50.4	-
CT3-800	25.116	27.215	35.302	0.198	0.177	0.224	41.1	46.1	37.2
CT4-800	25.316	27.277	35.376	0.244	0.224	0.277	33.3	36.5	30.1

D= crystallite size

Table 1 summarizes various parameters including the crystallite size of the CuO/TiO_2 nanoparticles as estimated by the Debye-Scherrer equation. It can be seen that the presence of the CuO in the samples influenced the shifting of the TiO_2 peaks to the left to slightly lower 2Θ degrees (Zhang et al., 2020). It is noticeable that the crystallite sizes of the samples calcined at 450 ℃ ranged from 8 nm to 12 nm. The crystallite sizes of the samples calcined at 600 ℃ were between 17-29 nm and 41-85 nm for the samples calcined at 800 ℃. The crystallite sizes of the CuO ranged from 27 nm to 39 nm. The crystallite sizes of the samples calcined at higher temperatures were relatively larger due to particle growth. The phase structure of the samples was further studied by the Raman spectroscopy. Figure 2 shows the Raman spectra of pure TiO_2 and CuO/TiO_2 samples sintered at 600 ℃ as representative samples. It can be seen that all samples reveal the existence of prominent Raman lines at 396, 516 and 639 cm^{-1} which are assignable to the B_1, B_{1g} and A_{1g} vibration modes of anatase TiO_2 crystal, respectively (Zhou et al. 2006, Peña-Flores et al. 2014). The Raman spectroscopy findings are in good agreement with the XRD results of the samples calcined at 600 ℃ as both reveal the formation of the prominent peaks of anatase TiO_2.

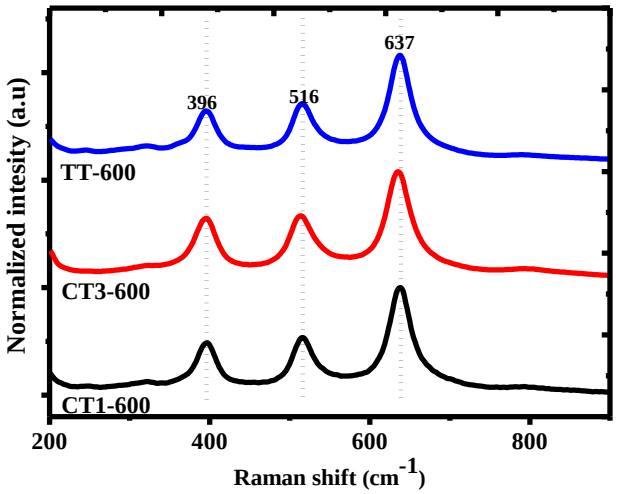

Figure 2: Raman spectra of the TT-600, CT1-600 and CT3-600 samples as representative samples.

The morphologies of the CuO/TiO_2 samples were examined by the SEM, TEM and high-resolution TEM analyses. The SEM was coupled with EDAX to investigate the elemental composition of the final products (Figure 3). The EDAX results show that the samples contain Ti, Cu and O. Figure 4A-D presents the SEM micrographs of the samples calcined at 600 ℃ while the images for the samples calcined at 800 ℃ are compiled in

Figure 4A-D. Figure 4A shows that the CT1-600 sample exhibited spherical aggregates with average diameter of 20-30 nm. On the other hand, samples with high content of CuO calcined 600 ℃ (CT2-600, CT3-600 and CT4-600) showed the existence of less aggregated and regular particles (Figure 4B-D).

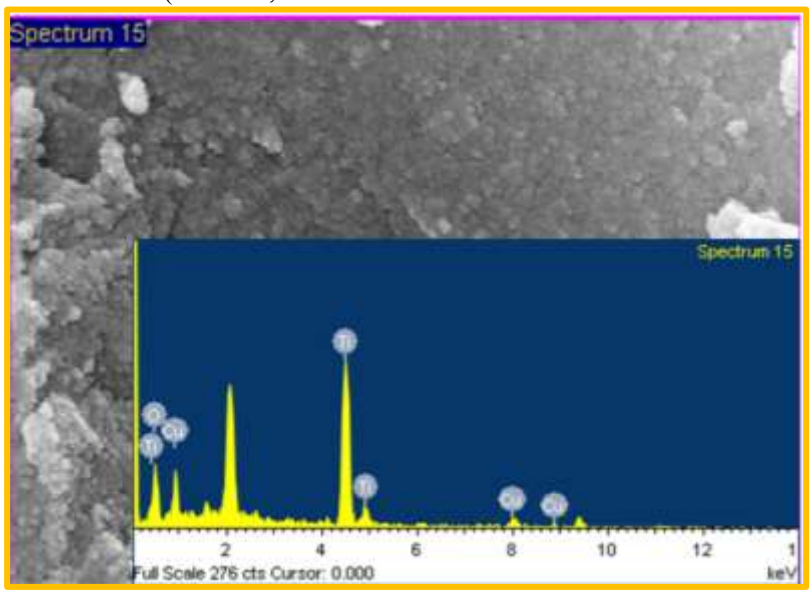

Figure 3: EDAX results of the CT2-600 as a representative sample showing the presence of Ti, Cu and O elements.

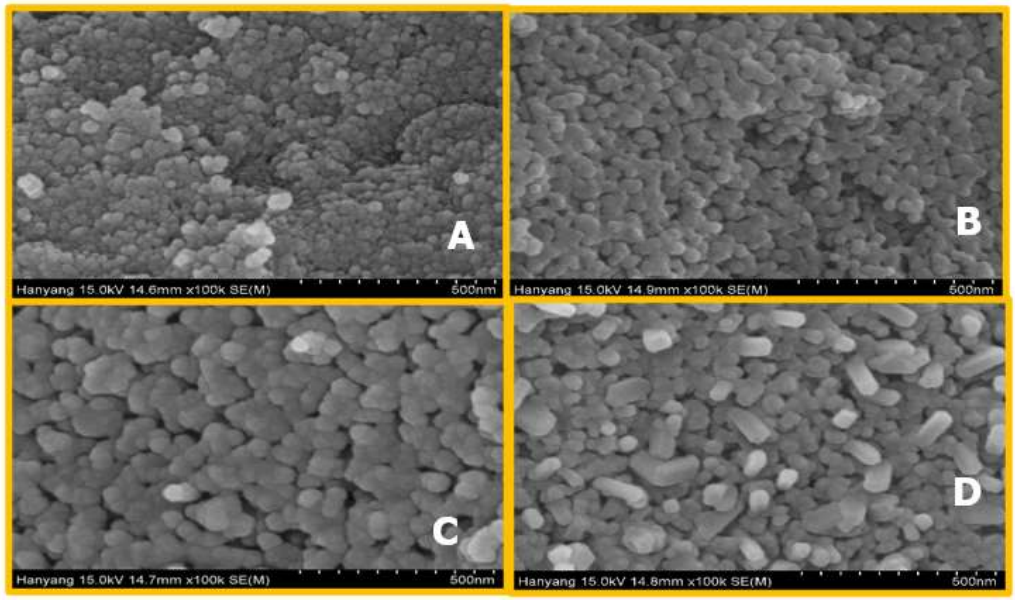

Figure 4: SEM micrographs of the CuO/TiO_2 samples calcined 600 ℃; CT1-600 (A), CT2-600 (B), CT3-600 (C), and CT4-600 (D).

The CT2-600 sample shows that the average diameter of the particles is less than 40 nm. The CT4-600 shows the existence of both rod-like and spherical particles. Generally, the samples obtained at 600 ℃ had a diameter less than 50 nm. Figure 5A-D presents the SEM images of the CuO/TiO_2 samples calcined 800 ℃. It is noticeable that the CuO/TiO_2 samples calcined at 800 ℃ exhibited a porous structure with a relatively increased particle size as a result of densification and coarsening. It can be seen that the particle size of these samples are between 50-60 nm.

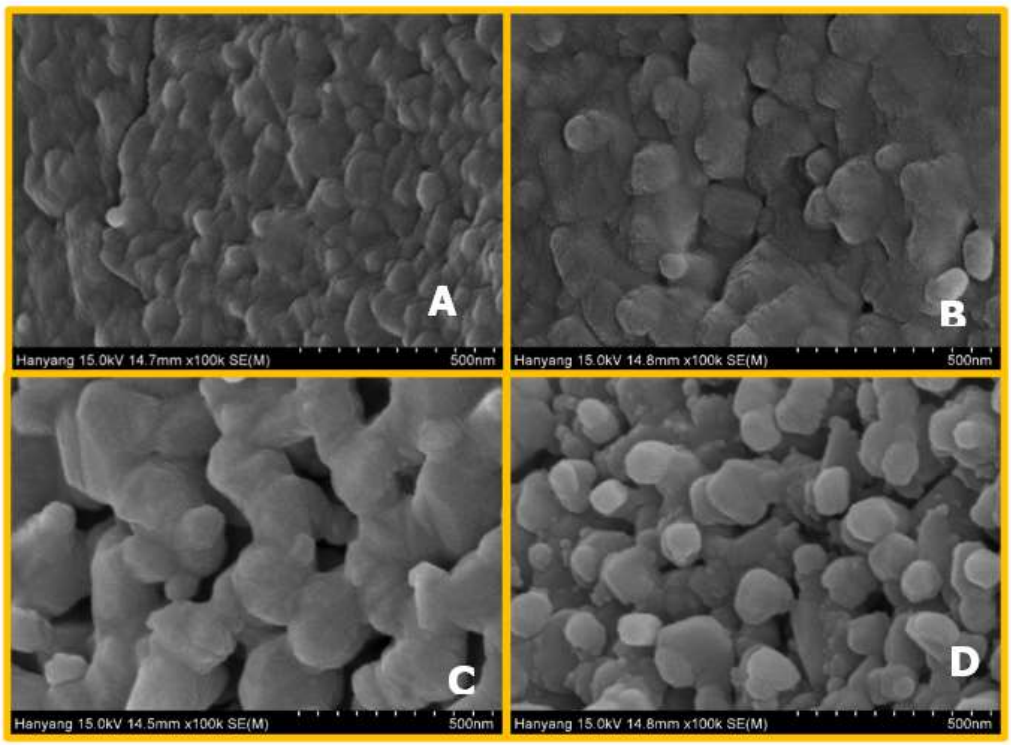

Figure 5: SEM micrographs of the CuO/TiO_2 samples calcined 800 ℃; CT1-800 (A), CT2-800 (B), CT3-800 (C), and CT4-800 (D).

Figure 6 compiles the TEM images of the CuO/TiO_2 of the samples calcined 600 ℃. It can be seen that the particle size of the CT-600 sample was approximately 20 nm (Figure 6A) while other samples (Figure 6B-D) show that the particle sizes are 20-40 nm. Figure 7 shows high-resolution TEM images of the CuO/TiO_2 samples calcined at 600 ℃. The lattice fringes of anatase TiO_2 crystals (0.36 nm) can clearly be seen (Figure 7A and B). Figure 7C and D reveals that in addition to the lattice fringes for anatase phase, the CT3-600 and CT4-600 samples show the lattice fringes for CuO (0.25 nm) indicating the interaction of CuO and TiO_2 (Abidi, et al., 2020). HR-TEM results are in good agreement with the XRD results (Figure 1C) demonstrating that the proposed preparation method is essential for formation of CuO/TiO_2 nanoparticles with well-developed crystal structure.

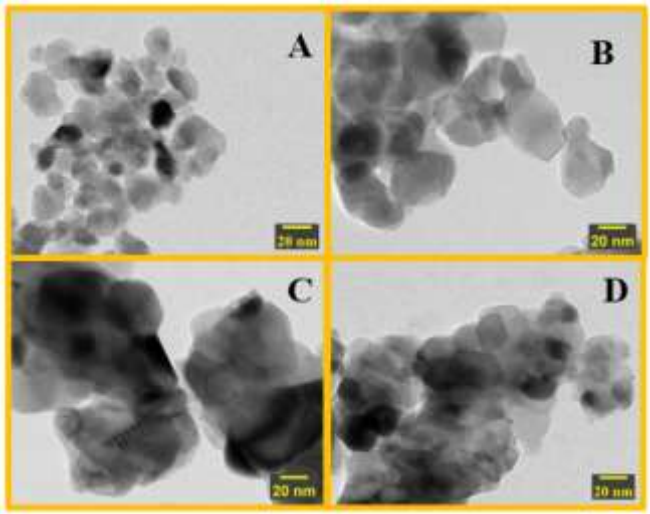

Figure 6: TEM images of the CuO/TiO_2 samples calcined 600 ℃; CT1-600 (A), CT2-600 (B), CT3-600 (C), and CT1-600 (D).

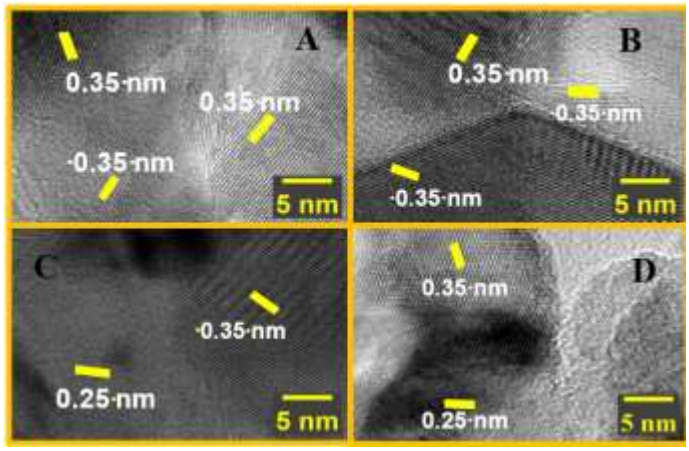

Figure 7: High resolution-TEM images of the CuO/TiO_2 samples calcined 600 ℃; CT1-600 (A), CT2-600 (B), CT3-600 (C), and CT4-600 (D).

The interaction between Cu and Ti in the CuO/TiO_2 samples was studied by UV-visible diffuse reflectance spectroscopy (UV-vis DRS). The reflectance spectra were transformed to Kubelka-Munk coordinates (KM, α) and then Tauc's plots were constructed from $(KM.\ h\upsilon)^{½}$ against hυ. The indirect band gap energies were estimated by extrapolating the linear portion of the Tauc's plots onto the hυ axis (Yu et al. 2011, Choudhury et al. 2013). Figure 8 compiles the UV-visible DRS spectra and their corresponding Tauc's plots of the samples calcined at 600 and 800 °C. It was previously reported that the absorption of the CuO/TiO_2 in the visible region is associated with the charge transfer from TiO_2 to CuO (Choudhury et al. 2013). Figure 8A reveals that pure TT-600 reveal a strong absorption at wavelength below 410 nm attributable to ligand-to-metal charge transfer between the O^{2-} ligand and the Ti^{4+} ion (Gutiérrez et al. 2006, Shao et al. 2015). On the other hand, Figure 8A and B show that the CuO/TiO_2 samples demonstrate the absorption edge at $\lambda \geq 575$ nm which covers the visible light region

(Pelaez, et al., 2012, Qu et al. 2012, Choudhury et al. 2013, Peña-Flores et al. 2014). Figure 8C indicates that the band gap energy registered by the TT600 sample was ~ 3.14 eV which is the typical band gap energy for the anatase structure. It can be observed that the band gap energies of the CuO/TiO_2 samples were below 3.0 eV. The CuO incorporated TiO_2 samples calcined at 600 ℃ had band gap energies ~1.6- 2.3 eV while the samples calcined at 800 ℃ registered band gap energies between 2.7-2.9 eV (Figure 8D). XRD results indicated that samples calcined at 600 ℃ exhibited smaller particles (~17-29 nm) than the samples calcined at 800 ℃ (~33-42 nm). Hence, the optical properties of the samples sintered at 600 ℃ were significantly improved due to quantum efficiency. The UV-visible DRS results indicate that the incorporation of CuO into the TiO_2 microstructure leads to shifting of the absorption properties to longer wavelengths and reduce the band gap of TiO_2 as well. Therefore, the samples obtained by this preparation method can essentially be used as heterogeneous photocatalysts due to their desirable optical properties (Choudhury et al., 2013, Peña-Flores et al. 2014, Abidi et al. 2020).

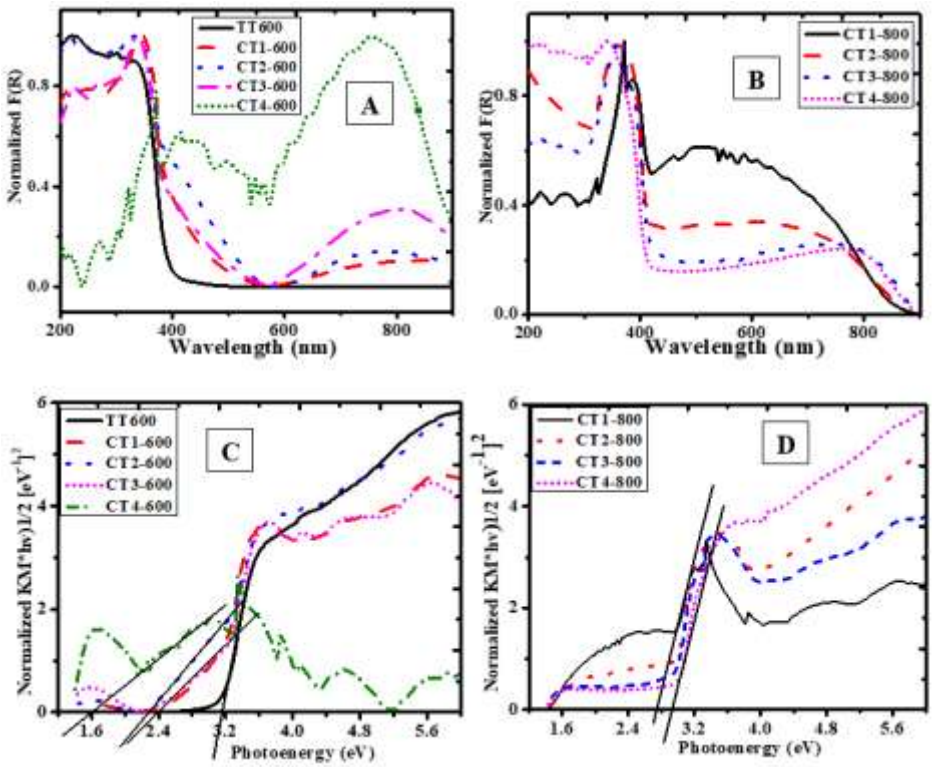

Figure 8: DRS spectra (A and B) and their respective band gap plots (C and D) of the CuO/TiO_2 samples calcined at 600 ℃ (A and C) and 800 ℃ (B and D).

The XPS analysis was performed to investigate the chemical states of the CuO/TiO_2 samples. The survey of the CuO/TiO_2 representative sample is presented in Figure 9. The characteristic peaks for Ti 2s, Ti 2p, Cu 2p and O 1s core level binding energies can be seen. Figure 9A shows the peak at 283.6 eV corresponding to the surface carbon (extraneous carbon) of the powdered samples (López and Llanos 2009, Wang et al. 2017). The peak correspond to O 1s can be seen at 527.9 eV (Figure 9B). The peak for Ti $2p_{1/2}$ can be observed at 462.2 eV while the peak at 456.3 is ascribed to Ti $p_{3/2}$ (Figure

9C). These significant peaks reveal the existence of Ti^{4+} states in the system. On the other hand, the peaks for the Cu $2p_{1/2}$ and Cu $p_{3/2}$ can be observed at 950.6 and 930.6 eV, respectively.

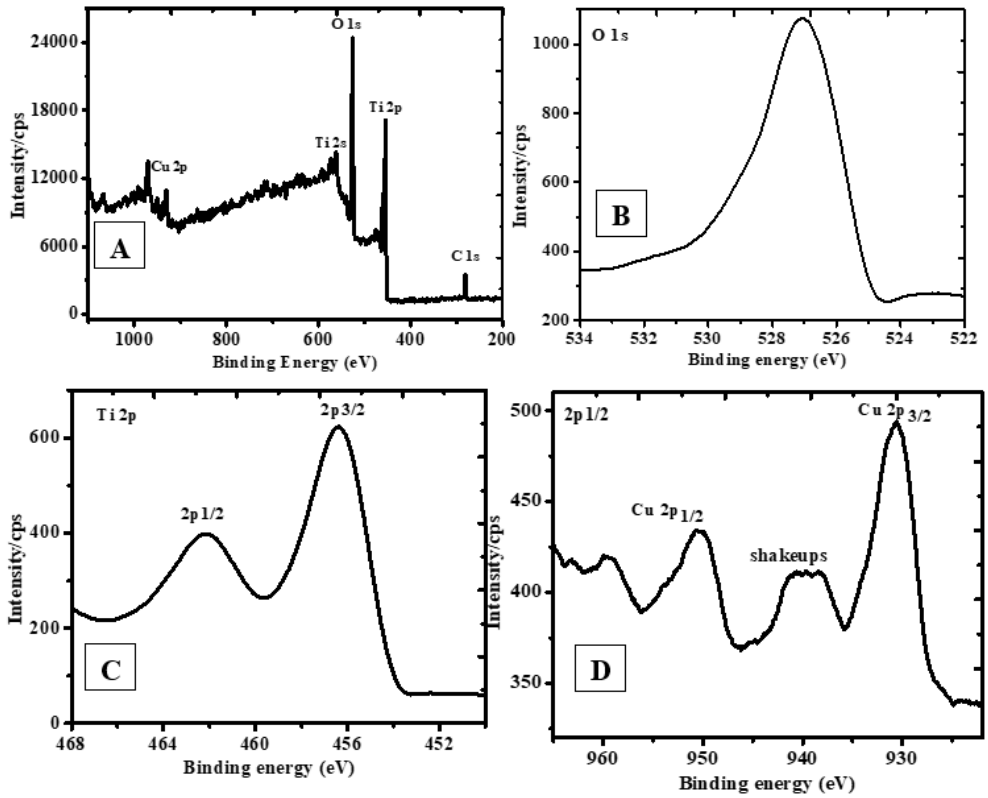

Figure 9: XPS spectra of CT2-600 as a representative sample of CuO/TiO_2 showing the presence of Ti, Cu and O in the sample.

This demonstrates that the CuO was incorporated into TiO_2 to form a composite (Figure 9D). The depiction of the satellite peaks at 960 eV and 936.8 eV indicates that the CuO was of Cu^{2+} species (Scoca et al. 2020, Zhang et al. 2020). These peaks have been reportedly to be caused by the oxidation of Cu^{+} species and they are normally absent in samples containing Cu_2O systems (Wang et al. 2017, Wang et al. 2023). This demonstrates that the obtained materials contained Ti, Cu and O elements. The shifting of the $Ti2p_{1/2}$ and O 1s peaks to lower binding energies has reportedly to be caused by the strong interaction between TiO_2 and CuO nanoparticles to form CuO/TiO_2 systems (Yuan et al. 2018, Baig et al. 2020).

The nitrogen gas adsorption-desorption studies were employed to study the textural properties of the CuO/TiO_2 samples at 77 K. Figure 10 and Table 2 show the nitrogen gas physisorption results of CT2-450, CT4-450, CT2-600 and CT4-600 as the representative samples. It can be seen that the samples depicted different textural properties depending on the CuO content and calcination temperatures. Table 2 indicates that the specific surface areas of the samples were between 18.5 and 109 m^2/g. The CuO/TiO_2 samples calcined at 450 °C had larger specific surface areas than the samples calcined at 600 °C. A drastic decrease of surface areas observed is due to crystallization upon calcination of the samples.

Table 2: Textural properties of the calcined CuO/TiO_2 samples

Sample name	Surface area (m^2 /g)	Pore volume (cm^3/g)	Pore diameter (nm)	Isotherm type	Hysteresis loop
CT2-450	109.0	0.299	10.7	IV	H2
CT4-450	88.6	0.155	8.2	IV	H2
CT2-600	30.4	0.184	76.5	IV	H3
CT4-600	18.5	0.053	119.5	IV	H3

The pore diameters of the samples calcined at 600 ℃ were larger than that of the samples calcined at 450 ℃. Figure 10A reveals that all samples except CT4-600 possessed Type IV isotherm curves signifying the presence of mesopores associated with capillary condensation of the adsorbent (Yao et al. 2009, Hilonga et al. 2010, Shao et al. 2015a). The nitrogen gas uptake of the CT1-450 and CT2-450 samples is centered at relative pressures of $0.4<P/Po<0.90$ signifying the presence of mesopores. The CT2-600 and CT4-600 samples demonstrated isotherm with a sharp uptake at $P/P_0 \geq 0.85$ indicating the presence of some macropores. The classification of the nitrogen gas physisorption isotherms of porous materials and their corresponding hysteresis loops has been reported. In the present study, the description of the hysteresis loops based on the classification provided by the IUPAC system as reported by Pierotti and Rouquerol (1985) and Sing and Williams (2004). It is noticeable that the CT2-450 and CT4-450 samples depict the hysteresis loops that are very similar to type H2 according to the IUPAC classification systems portraying the presence of aggregates with channel-like pores. The CT2-600 and CT4-600 samples possessed a type H3 hysteresis loop indicating the presence of aggregates of plate-like particles or the assemblage of slit-shaped pores (Cao et al.2009, Hilonga et al., 2010, Park and Shao 2019). It was previously reported that in a system exhibiting type H2 or H3 hysteresis there is an existence of random distribution of pores and interconnected pore system (Hilonga, et al., 2010).

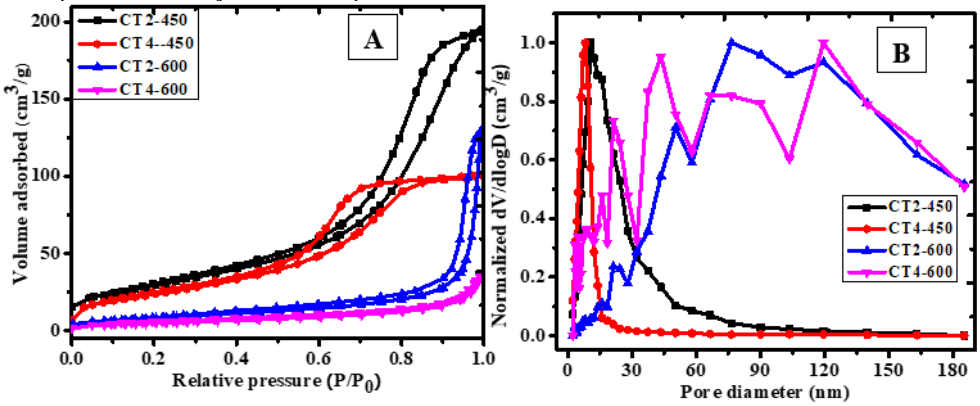

Figure 10: Nitrogen gas adsorption-desorption isotherms (A) and pore size distribution (B) for the CuO/TiO_2 samples calcined 450 ℃ and 600 ℃ as representative samples.

Figure 10B displays the pore size distribution (PSD) of both samples calcined at 450 and 600 °C. It can be seen that the CT2-450 and CT4-450 samples demonstrated a narrow PSD between 4 and 35 nm. On the other hand, the CT2-600 and CT4-600

samples showed broad PSD from 5-150 nm implying the presence of mesopores and macropores (Yao et al. 2009, Shao et al. 2013). The nitrogen gas physisorption studies indicated that the calcination temperature can adversely decrease the surface area of the samples and increase their pore diameter.

The modification of TiO_2 with metal oxides has reportedly to yield metal oxides with improved morphology, crystal structure and optical properties (Zhou et al. 2006, Pelaez et al. 2012, Tobaldi et al. 2013). Structural characterizations demonstrated that the introduction of CuO into TiO_2 has a profound effect on the physico-chemical properties of the final products. XRD results indicated that CuO/TiO_2 final products with only anatase, rutile TiO_2 crystals or a mixture of both anatase and rutile can be yielded by varying the calcination temperature and CuO content. Phase transformation in pure TiO_2 and titania-based materials has been widely studied. The ART is reported to be affected by the preparation method, presence of impurities, particle size, and calcination temperature (Scoca et al. 2020, Song et al. 2020, Zhang et al. 2020). The phase transformation process involves the nucleation of the rutile phase at the anatase 112 twin boundary caused by the low activation barrier. The nucleation results through the breaking of the Ti-O bonds and eventual rearrangement of Ti atoms in the unit cell. This process is feasible since the anatase is thermodynamically metastable phase of TiO_2 thus it can irreversibly transform to rutile phase. The ART is a nucleation and growth dependent process as it can be affected by morphology, particle size, calcination temperature, impurities, synthetic process etc. (Hanaor and Sorrell 2011, Song et al. 2020). The role played by cationic species such as Cu^{2+} in promoting the ART has been explained by the ionic radii-valance concept. It is assumed that the cations with small radii and low valence can substitute and eventually occupy the lattice sites of Ti^{4+} ions. This process increases the number of oxygen vacancies and accelerate the ART (Hanaor and Sorrell 2011, Prajapat et al. 2024). The ionic radius of Cu^{2+} (0.68 Å) is very close to the ionic radius of Ti^{4+} (0.65 Å) hence the ionic substitution is possible (Xu et al. 2018, Prajapat et al. 2024). SEM results showed that the introduction of the CuO into TiO_2 microstructure and subsequent calcination of the as-prepared samples influence their particle size and shape. Calcination of the as-prepared samples led to the formation of a porous structure with less aggregated and regular particles. It was also observed that the shape of the particles was also influenced by calcination temperatures as the samples revealed the existence of spherical particle to rod-like particles (CT4-600).

It was further observed that the band gap energies of the obtained nanoparticles were reduced due to the incorporation of CuO into TiO_2 microstructure. Studies have pointed out that the introduction of the Cu^{2+} ions creates new energy levels at the band of TiO_2. Thus, the energy required to excite electron from the valance band to the conduction band is essentially reduced (Prajapat et al. 2024). Therefore, the single step sol-gel method proposed by present study is convenient and suitable for the formation of CuO/TiO_2 systems with improved physicochemical properties in the absence of additives. The proposed technique is unique and is expected to encourage industrial and large-scale production of CuO/TiO_2 nanoparticles with superior properties for heterogeneous photocatalysis.

Conclusions

In the present report the CuO/TiO_2 systems were exquisitely prepared and their microstructure was studied using various characterization methods. The samples were synthesized by a versatile and cost-effective single step sol-gel approach using titanium oxychloride as a TiO_2 source in the absence of additive. Structural characterizations of the CuO/TiO_2 systems demonstrated that samples with different physicochemical properties can be obtained depending on the CuO content and the calcination temperature. XRD analysis showed that the presence of the CuO delayed the anatase to rutile phase transformation at high calcination

temperatures. SEM and high-resolution TEM results showed that samples with less aggregated particles were produced. Thus, the suggested preparation method facilitated the formation of CuO/TiO_2 samples with superior properties (phase structure, crystallinity, crystallite size, morphology and porous structure). The synthetic method introduced in this study is expected to enhance the large-scale industrial production of cost-effective CuO/TiO_2.

References

Abidi M, Hajjaji A, Bouzaza A, Trablesi K, Makhlouf H, Rtimi S, Assadi A, and Bessais B. 2020 Simultaneous removal of bacteria and volatile organic compounds on Cu_2O-NPs decorated TiO_2 nanotubes: competition effect and kinetic studies. *J. Photochem. Photobiol. A: Chem.* 400: 112722.

Anpo M and Takeuchi M 2003 The design and development of highly reactive titanium oxide photocatalysts operating under visible light irradiation. *J. Catal. 216*(1–2):, 505-516.

Baig, U, Ansari, MA, Gondal, M, Akhtar, S, Khan, FA and Falath, W. (2020). Single step production of high-purity copper oxide-titanium dioxide nanocomposites and their effective antibacterial and anti-biofilm activity against drug-resistant bacteria. *Mater. Sci. Eng. C.* 113: 110992.

Baran AE, Ates S, Sığırcık G 2022 CuO-TiO_2 nanostructures prepared by chemical and electrochemical methods as photo electrode for hydrogen production. *Int. J. Hydrogen Energy. 47*(10): 6519-6534.

Cao S, Yeung KL, Kwan JKC, To, PMT and Yu SCT 2009 An investigation of the performance of catalytic aerogel filters. *Appl. Catal. B.* 86(3–4): 127-136.

Chiarello GL, Selli E and Forni L. 2008 Photocatalytic hydrogen production over flame spray pyrolysis-synthesised TiO_2 and Au/TiO_2. *Appl. Catal. B* . 84(1–2): 332-339.

Choudhury B., Dey M, Choudhury A 2013 Defect generation, d-d transition, and band gap reduction in Cu-doped TiO_2 nanoparticles. *Int. Nano Lett.* 3(1): 25.

Clarizia L, Spasiano D, Di Somma I, Marotta R, Andreozzi R and Dionysiou DD 2014 Copper modified-TiO2 catalysts for hydrogen generation through photoreforming of organics. A short review. *Int. J. Hydrog. Energy*, 39(30): 16812-16831.

Comini E, BarattoC, Faglia G, Ferroni M, Vomiero A and Sberveglieri G 2009 Quasi-one dimensional met al oxide semiconductors: Preparation, characterization and application as chemical sensors. *Progress Math. Sci.* 54(1): 1-67.

Etape EP, Ngolui LJ, Foba-Tendo J, Yufanyi DM, Namondo BV 2017 Synthesis and characterization of CuO, TiO_2, and CuO-TiO_2 mixed oxide by a modified oxalate route. *J. Appl. Chem. 2017*: 1-10.

Gutiérrez OY, Fuentes GA, Salcedo C and Klimova T 2006 SBA-15 supports modified by Ti and Zr grafting for NiMo hydrodesulfurization catalysts. *Catal. Today*, 116(4): 485-497.

Hanaor DA and Sorrell CC 2011 Review of the anatase to rutile phase transformation. *J. Mater. Sci.* 46(4): 855-874.

Hilonga A, Kim JK, Sarawade P and Kim H 2010 Mesoporous titania–silica composite from sodium silicate and titanium oxychloride. Part I: grafting method. *J. Mater. Sci.* 45(5): 1255-1263.

Kim YN, Shao GN, Jeon SJ, Imran SM, Sarawade PB, Kim HT 2013 Sol–gel synthesis of sodium silicate and titanium oxychloride based TiO_2–SiO_2 aerogels and their photocatalytic property under UV irradiation. *Chem. Eng. J.* 231 (2013) 502-511.

Li Z, Ding D, Liu Q, Ning C and Wang X 2014 Ni-doped TiO_2 nanotubes for wide-range hydrogen sensing. *Nanoscale Res. Lett.* 9(1): 118.

Lin JCT, Sopajaree K, Jitjanesuwan T and Lu MC 2018 Application of visible light on copper-doped titanium dioxide catalyzing degradation of chlorophenols. *Separ. Purif. Technol.* 191: 233-243.

López R, Gómez R and Llanos ME 2009 Photophysical and photocatalytic

properties of nanosized copper-doped titania sol–gel catalysts. *Catal. Today,* 148(1-2): 103-108.

Moniz SJA and Tang J 2015 Charge Transfer and Photocatalytic Activity in CuO/TiO_2 Nanoparticle Heterojunctions Synthesised through a Rapid, One-Pot, Microwave Solvothermal Route. *ChemCatChem.* 7(11): 1659-1667.

Mutuma BK, Shao GN, Kim WD and Kim HT 2015 Sol–gel synthesis of mesoporous anatase–brookite and anatase–brookite–rutile TiO_2 nanoparticles and their photocatalytic properties. *J. Colloid Interface Sci.* 442(0): 1-7.

Nakata, K., & Fujishima, A. (2012). TiO2 photocatalysis: Design and applications. *J. Photochem. Photobiol. C: Photochem. Rev. 13*(3): 169-189. doi: http://dx.doi.org/10.1016/j.jphotochemrev.2012.06.001

Park S and Shao G 2019 Microstructure and materials characterization of sol-gel synthesized ZrO_2 systems. *Tanzania J. Sci.* 45(2): 190-208.

Pelaez M, Nolan NT, Pillai SC, Seery MK, Falaras P, Kontos AG, Dunlop PS, Hamilton JW, Byrne JA and O'Shea K 2012 A review on the visible light active titanium dioxide photocatalysts for environmental applications. *Appl. Catal. B.*125: 331-349.

Peña-Flores JI, Palomec-Garfias AF, Márquez-Beltrán C, Sánchez-Mora E, Gómez-Barojas E and Pérez-Rodríguez F. 2014 Fe effect on the optical properties of TiO_2: Fe_2O_3 nanostructured composites supported on SiO_2 microsphere assemblies. *Nanoscale Res. Lett.* 9(1): 1-7.

Pierotti, R., & Rouquerol, J. (1985). Reporting physisorption data for gas/solid systems with special reference to the determination of surface area and porosity. *Pure App.l Chem.* 57(4): 603-619.

Prajapat K, Mahajan U, Dhonde M, Sahu K, Shirage P 2024 Synthesis and characterization of TiO_2 nanoparticles: unraveling the influence of copper doping on structural, surface morphology, and optical properties. *Chem. Phys. Impact*. (2024): 100607.

Qu Y, Zhou W, Ren Z, Du S, Meng X, Tian G, Fu H 2012 Facile preparation of porous $NiTiO_3$ nanorods with enhanced visible-light-driven photocatalytic performance. *J. Mater. Chem. 22*(32):16471-16476.

Ravishankar T, Vaz MDO, Teixeira S 2020 The effects of surfactant in the sol–gel synthesis of CuO/TiO_2 nanocomposites on its photocatalytic activities under UV-visible and visible light illuminations. *New J. Chem.* 44(5):1888-1904.

Scoca DL, Cemin F, Bilmes SA, Figueroa CA, Zanatta AR, Alvarez F 2020 Role of rare earth elements and entropy on the anatase-to-rutile phase transformation of TiO_2 thin films deposited by ion beam sputtering. *ACS Omeg.* 5(43): 28027-28036.

Shao GN, Elineema G, Quang DV, Kim YN, Shim YH, Hilonga A, Kim JK and Kim HT. 2012 Two step synthesis of a mesoporous titania–silica composite from titanium oxychloride and sodium silicate. *Powder Technol.* 217(0): 489-496.

Shao GN, Engole M, Imran SM, Jeon SJ and Kim HT 2015 Sol–gel synthesis of photoactive kaolinite-titania: Effect of the preparation method and their photocatalytic properties. *Appl. Surf. Sci.* 331(0): 98-107.

Shao GN, Hilonga A, Kim YN, Kim JK, Elineema G, Quang DV, Jeon SJ and Kim HT 2012a Peptization technique in the synthesis of titania–silica composites and their photocatalytic properties. *Chem. Eng. J.* 198–199(0): 122-129.

Shao GN, Imran SM, Jeon SJ, Kang SJ, Haider SM and Kim HT 2015a Sol–gel synthesis of vanadium doped titania: Effect of the synthetic routes and investigation of their photocatalytic properties in the presence of natural sunlight. *Appl. Surf. Sci.* 351: 1213-1223.

Shao GN, Jeon SJ, Haider MS, Abbass N and Kim HT 2016 Investigation of the influence of vanadium, iron and nickel dopants on the morphology, and crystal

structure and photocatalytic properties of titanium dioxide based nanopowders. *J. Colloid. Interface Sci.* 474: 179-189.

Shao GN, Hilonga A, Jeon SJ, Lee JE, Elineema G, Quang DV, Kim JK and Kim HT 2013 Influence of titania content on the mesostructure of titania–silica composites and their photocatalytic activity. *Powder Technol.* 233(0): 123-130.

Shao GN, Kim Y, Imran SM, Jeon SJ, Sarawade PB, Hilonga A, Kim JK and Kim HT 2013a Enhancement of porosity of sodium silicate and titanium oxychloride based TiO_2–SiO_2 systems synthesized by sol–gel process and their photocatalytic activity. *Micropor. Mesopor. Mater.* 179(0): 111-121.

Sing, K. S., & Williams, R. T. (2004). Physisorption hysteresis loops and the characterization of nanoporous materials. *Adsorpt. Sci. Technol.* 22(10): 773-782.

Singh DP, Ojha AK, Srivastava ON 2009 Synthesis of different $Cu(OH)_2$ and CuO (nanowires, rectangles, seed-, belt-, and sheetlike) nanostructures by simple wet chemical route. *J. Phys. Chem. C.* 113(9): 3409-3418.

Song M, Lu Z, Li D 2020 Phase transformations among TiO_2 polymorphs. *Nanoscale.* 12(45): 23183-23190.

Tan LL, Ong WJ, Chai SP and Mohamed AR 2016 Visible-light-activated oxygen-rich TiO_2 as next generation photocatalyst: Importance of annealing temperature on the photoactivity toward reduction of carbon dioxide. *Chem. Eng. J.* 283: 1254-1263.

Tanemura S, Miao L, Jin P, Kaneko K, Terai A, Nabatova-Gabain N 2003 Optical properties of polycrystalline and epitaxial anatase and rutile TiO_2 thin films by rf magnetron sputtering. *Appl. Surf. Sci.* 212–213(0): 654-660.

Thongpool V, Phunpueok A, Jaiyen S and Sornkwan T 2020 Synthesis and photocatalytic activity of copper and nitrogen co-doped titanium dioxide nanoparticles. *Results Phys.* 16: 102948.

Tobaldi DM, Sever Škapin A, Pullar RC, Seabra MP and Labrincha JA 2013 Titanium dioxide modified with transition metals and rare earth elements: Phase composition, optical properties, and photocatalytic activity. *Ceram. Int.* 39(3): 2619-2629.

Wang X, Xu G, Zhou Z, Qin X, Su Y, Zhang X, Wu W 2023 Cu_2O@TiO_2 core-shell microspheres for naphthalene oxidation. *J. Porous Mater.* 30(4): 1295-1302.

Wang Y, Tao J, Wang X, Wang Z, Zhang M, He G and Sun Z 2017) A unique Cu_2O/TiO_2 nanocomposite with enhanced photocatalytic performance under visible light irradiation. *Ceram. Int.* 43(6): 4866-4872.

Xu L, Zheng G, Pei S, Wang J 2018 Investigation of optical bandgap variation and photoluminescence behavior in nanocrystalline CuO thin films. *Optik. 158*: 382-390.

Yao N, Cao S andYeung KL 2009 Mesoporous TiO_2–SiO_2 aerogels with hierarchal pore structures. *Microporor. Mesopor. Mater.* 117(3): 570-579.

Yu J, Hai Y, Jaroniec M 2011 Photocatalytic hydrogen production over CuO-modified titania. *J. Colloid Interface Sci.* 357(1): 223-228.

Yuan J, Zhang JJ, Yang MP, Meng WJ, Wang H, Lu JX 2018 CuO nanoparticles supported on TiO_2 with high efficiency for CO_2 electrochemical reduction to ethanol. *Catalysts:* 8(4): 171.

Zaleska, A 2008 Doped-TiO_2 a review. *Recent Patents Eng.* 2(3):157-164.

Zeng Y, Wang T, Zhang S, Wang Y, Zhong Q 2017 Sol–gel synthesis of CuO-TiO_2 catalyst with high dispersion CuO species for selective catalytic oxidation of NO. *Appl. Surf. Sci.* 411: 227-234.

Zhang S, Gong X, Shi Q, Ping G, Xu H, Waleed A, Li G 2020 CuO nanoparticle-decorated TiO_2-nanotube heterojunctions for direct synthesis of methyl formate via photo-oxidation of methanol. *ACS Omega.* 5(26): 15942-15948.

Zhou J, Zhang Y, Zhao XS and Ray AK 2006 Photodegradation of Benzoic Acid

over Metal-Doped TiO_2. *Ind. Eng. Chem. Res.* 45(10): 3503-3511.